Molecular Therapy
Nucleic Acids
Original Article

miR-181a, delivered by hypoxic PTC-secreted exosomes, inhibits DACT2 by downregulating MLL3, leading to YAP-VEGF-mediated angiogenesis

Yingxue Wang,[1] Aiying Cen,[1] Yuxian Yang,[2] Huilin Ye,[3] Jiaying Li,[1] Shiliang Liu,[2] and Lei Zhao[2]

[1]Department of Endocrinology, the First Affiliated Hospital of Jinan University, Guangzhou 510630, P.R. China; [2]Department of Radiation Oncology, Sun Yat-sen University Cancer Center, State Key Laboratory of Oncology in South China, Collaborative Innovation Center for Cancer Medicine, Guangzhou 510060, P.R. China; [3]Department of Hepatopancreatobiliary Surgery, Sun Yat-sen Memorial Hospital, Sun Yat-sen University, Guangdong Provincial Key Laboratory of Malignant Tumor Epigenetics and Gene Regulation, Guangzhou 510120, P.R. China

Papillary thyroid cancer (PTC) is the most common type of thyroid cancer, and angiogenesis plays critical roles in its recurrence and metastasis. In this study, we investigated the effects of hypoxia-induced exosomal microRNA-181 (miR-181a) from PTC on tumor growth and angiogenesis. Thyroid-cancer-related differentially expressed miR-181a was identified by microarray-based analysis in the Gene Expression Omnibus (GEO) database. We validated that miR-181a was highly expressed in PTC cells and even more so in cells cultured under hypoxic conditions, which also augmented exosome secretion from PTC cells. Exosomes extracted from PTC cells with manipulated miR-181a and mixed-lineage leukemia 3 (MLL3) were subjected to normoxic or hypoxic conditions. Human umbilical vein endothelial cells (HUVECs) were transfected with miR-181a inhibitor/mimic or small interfering RNA (siRNA)-MLL3 or treated with exosomes from hypoxic PTC cells. Hypoxic exosomal miR-181a delivery promoted proliferation and capillary-like network formation in HUVECs. Mechanistically, miR-181a targeted and inhibited MLL3. Furthermore, miR-181a downregulated DACT2 and upregulated YAP and vascular endothelial growth factor (VEGF). Further, hypoxic exosomal miR-181a induced angiogenesis and tumor growth *in vivo*, which was reversed by hypoxic exosomal miR-181a inhibitor. In conclusion, exosomal miR-181a from hypoxic PTC cells promotes tumor angiogenesis and growth through MLL3 and DACT2 downregulation, as well as VEGF upregulation.

INTRODUCTION

Papillary thyroid cancer (PTC) is the most common type of thyroid malignancy.[1] The morbidity of PTC worldwide is increasing, and metastatic events to lymph nodes are frequently occurring for PTC, which is involved with tumor cell proliferation and angiogenesis.[2] Despite optimized current treatments, which include surgery, radioiodine therapy, and thyroid-stimulating hormone suppression and depletion, metastatic and aggressive spread occurs in approximately 5% of the PTC patients.[3] Emerging studies have proposed novel anticancer biomarkers in PTC, which may provide new potential for treating patients with progressive disease.[4] The lack of well-tolerated drugs and limited data about the pathophysiological processes involved in metastatic thyroid cancer calls for further efforts toward developing new biomarkers and treatments. Interestingly, exosomes (EXs) secreted by cancer cells cultured under hypoxic conditions load with non-coding microRNAs (miRNAs) implicated in the interplay of cancer and para-carcinoma cells, thus contributing to angiogenesis of the tumor microenvironment.[5]

EXs are small membranous vesicles, which are involved in various biological processes such as endothelial dysfunction and vascular remodeling.[6] EXs have been deciphered to participate in cellular communication through the shuttling of bioactive miRNAs, proteins, and mRNAs.[7] While miRNAs do not code for proteins, they can modulate expression of target proteins by regulating the degradation or translation of their targeted mRNA.[8] Emerging evidence shows that the progression and metastasis of PTC and other human cancers are mediated by dysregulation of miRNAs.[9] Here we noted that miR-181a has been extensively studied in a wide variety of human cancers, including breast,[10] cervical,[11] and gastric cancers.[12] A recent study has shown that miR-181a promotes cell proliferation and inhibits apoptosis in thyroid cancer,[13] and other research shows upregulation of miR-181a content in PTC cell-derived EXs.[14] In our study, TargetScan predicted histone-lysine N-methyltransferase-3 (MLL3, also known as lysine N-methyltransferase 2C or KMT2C) to be a target gene for miR-181a. MLL3, which belongs to the myeloid/lymphoid or mixed-lineage leukemia (MLL) family, participates in the development of various cancers.[15,16] MLL3 functions as an H3K4me1 methylase,[17] which other research indicates elevates the expression of disheveled binding antagonist of beta-catenin 2 (DACT2).[18,19] Vascular endothelial growth factor (VEGF) is a widely recognized trigger of angiogenesis

Received 3 August 2020; accepted 22 February 2021;
https://doi.org/10.1016/j.omtn.2021.02.027.

Correspondence: Lei Zhao, Department of Radiation Oncology, Sun Yat-sen University Cancer Center, State Key Laboratory of Oncology in South China, Collaborative Innovation Center for Cancer Medicine, No. 651, Dongfeng Road East, Guangzhou 510060, Guangdong Province, P.R. China.
E-mail: zhaolei@sysucc.org.cn

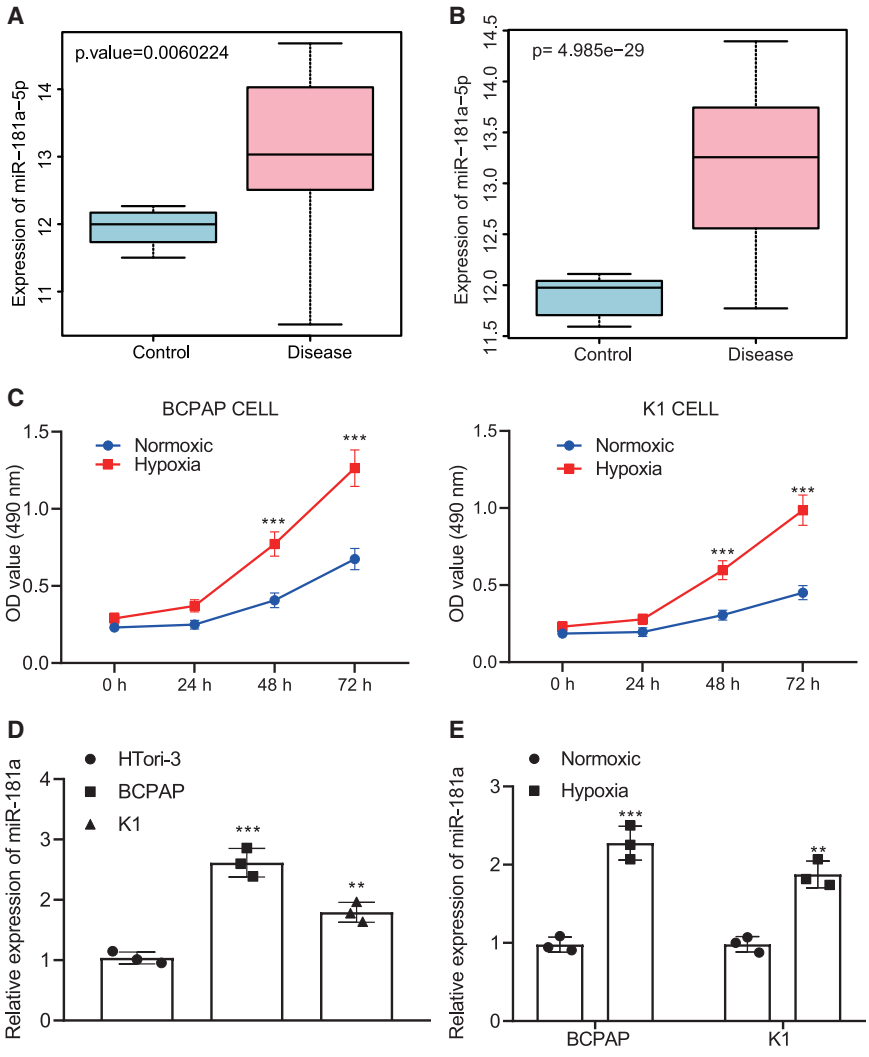

Figure 1. High miR-181a expression is observed in PTC cells cultured under hypoxia condition

(A and B) miR-181a-5p expression predicted in GEO: GSE103996 (A) and GSE73182 (B). The blue box on the left indicates the expression of normal samples, the red box on the right indicates the expression of thyroid cancer samples, and the upper left corner is the p value indicating the difference. (C) Cell viability under normoxic and hypoxic conditions analyzed by CCK-8 assay. (D) miR-181a expression in BCPAP, K1, and HTori-3 cells. (E) miR-181a expression in BCPAP and K1 cells after 24 h incubation under hypoxia. *p < 0.05, **p < 0.01, ***p < 0.001 versus control samples, normoxic BCPAP and K1 cells or HTori-3 cells. Data were presented as mean ± SD. Unpaired t test was used to compare two sets of data. One-way ANOVA with Tukey post hoc test was used to analyze data from multiple groups. Data comparison between groups at different time points was performed by two-way ANOVA, followed by Bonferroni post hoc test. The cell experiments were repeated in triplicate.

in the development of tumors,[20,21] and miR-181a can accelerate angiogenesis by activating the VEGF-related pathway in colorectal cancer.[22] Based on this background, we hypothesized that PTC cell-derived exosomal miR-181a might participate in angiogenesis in PTC via effects on the MLL3/DACT2/YAP-VEGF axis.

RESULTS

miR-181a is upregulated in PTC cells under hypoxia

To study the role of miRNAs in PTC, we conducted differential gene analysis of microarray data. Based on the analyses for miRNAs expression in datasets GSE73182 and GSE103996, miR-181a-5p was found to be highly expressed in thyroid cancer (Figures 1A and 1B). Hypoxia is one of important factors inducing tumor growth, so we further investigated effects of hypoxia on the PTC cells. Viability did not significantly differ between BCPAP and K1 cells under normoxia conditions versus hypoxia conditions at 24 h incubation. However, hypoxia increased cell viability at 48 and 72 h (Figure 1C). Moreover, quantitative real-time polymerase chain reaction (PCR) revealed that the miR-181a expression level was higher in BCPAP and K1 than that in the human normal thyroid cell line HTori-3 cultured in normoxic condition (Figure 1D). miR-181a expression level was further increased in BCPAP and K1 cells under hypoxia. Since the change of miR-181a expression in BCPAP cells was greater than that in K1 cells after induction of hypoxia (Figure 1E), we selected the BCPAP cells for further studies.

Hypoxia promotes secretion of PRKCD and transfer of exosomal miR-181a to HUVECs from BCPAP cells

To study the effect of hypoxia on the release of EXs from BCPAP cells, we incubated BCPAP cells with the same confluency under the condition of normoxia (20% O_2) and hypoxia (1% O_2). Electron microscopy examination showed that BCPAP cell-derived EXs were round, with diameters between 30 and 150 nm (Figures 2A and 2B). Nanoparticle tracking analysis (NTA) revealed that under normoxia and hypoxia conditions, EXs secreted by BCPAP cells were similar in size and distribution. However, the concentration of EXs from hypoxic BCPAP cells was higher than that from normoxic BCPAP cells (Figure 2C). In addition, western blot confirmed exosomal markers CD9, CD81, TSG101, HSP70, ALIX, and Flotillin-1 expression in BCPAP cell-derived EXs, which was higher under hypoxia, relative to the normoxia condition (Figure 2D). Therefore, hypoxia enhanced the secretion of BCPAP EXs.

Moreover, quantitative real-time PCR revealed that miR-181a expression was higher in hypoxic BCPAP cell-derived EXs than in normoxic BCPAP cell-derived EXs (Figure 2E). We then treated human umbilical vein endothelial cells (HUVECs) with hypoxic and

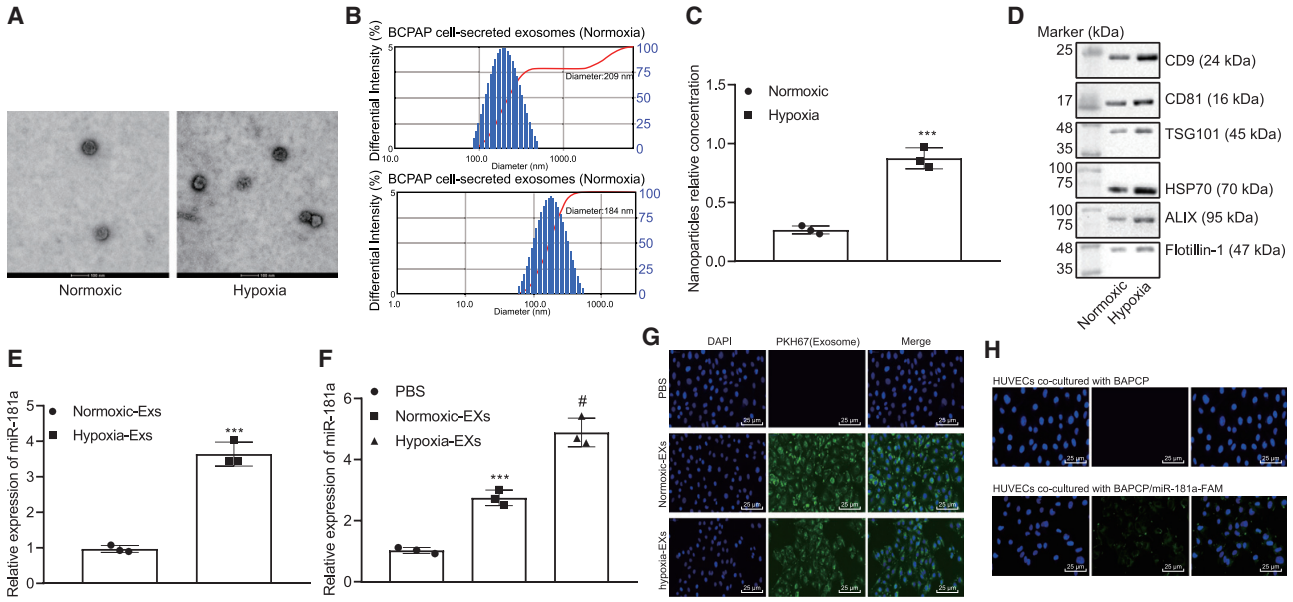

Figure 2. Hypoxia induces secretion of exosomes (EXs) and transportation of miR-181a via EXs to HUVECs from BCPAP cells

(A) Representative images showing the morphology of EXs by electron microscopy (scale bar, 100 nm). (B) Exosomal size, distribution, and concentration measured by nanoparticle tracking analysis. (C) Nanoparticle concentrations of EXs from normoxic and hypoxic BCPAP cells. (D) Exosomal markers analyzed by western blot. (E) miR-181a expression in EXs from normoxic and hypoxic BCPAP cells. (F) miR-181a expressions in HUVECs treated with EXs from normoxic and hypoxic BCPAP cells. (G) Representative images showing endocytosis of BCPAP cell-derived exos EXs omes by HUVECs via laser scanning confocal microscopy (LSCM; ×400). (H) Representative images of green fluorescence of HUVECs co-cultured with EXs from BCPAP cells treated with FAM-labeled miR-181a via LSCM (×400). *$p < 0.05$, **$p < 0.01$, ***$p < 0.001$ versus PBS-treated HUVECs, normoxic BCPAP cells, or normoxic-EXs. #$p < 0.05$ versus normoxic-EXs. Data were presented as mean ± SD. Unpaired t test was used to compare two sets of data. One-way ANOVA with Tukey post hoc test was used to analyze data from multiple groups. The cell experiments were repeated in triplicate.

normoxic BCPAP cell-derived EXs. Relative to treatment of PBS, the miR-181a expression was elevated in response to both normoxic and hypoxic BCPAP cell-derived EX treatment. Further, miR-181a expression was upregulated by hypoxic BCPAP cell-derived EX treatment compared with treatment by normoxic BCPAP cell-derived EXs (Figure 2F). Furthermore, confocal microscopy depicted that HUVECs could endocytose BCPAP cell-derived EXs (Figure 2G). In addition, after co-culture with BCPAP cells transfected with 3′ Carboxyfluorescein-tagged miR-181a, green fluorescence was observed in HUVECs by confocal microscopy (Figure 2H). These results demonstrated that miR-181a was transported from BCPAP cells to HUVECs through exosomes.

miR-181a overexpression promotes proliferation, migration, and network formation in HUVECs *in vitro*

To determine whether miR-181a affects proliferation, migration, and angiogenesis of HUVECs *in vitro*, we transfected HUVECs with miR-181a mimic or miR-181a inhibitor. In the preliminary experiments, we first set different concentrations of miR-181a mimic or miR-181a inhibitor to transfect HUVECs, and mimics and inhibitors at a concentration of 0 pmol were added as controls. The results showed that when the concentration of miR-181a inhibitors or mimics was higher than 100 pmol, the inhibition or increase of miR-181a expression by miR-181a inhibitors or mimics became stable (Figure S1). Therefore, 100 pmol inhibitors or mimics significantly suppressed or upregulated the expression of miR-181a, which was the most appropriate concentration for subsequent experiments. Further, miR-181a mimic expression was increased than that in mimic-NC, but miR-181a inhibitor reduced miR-181a expression in HUVECs relative to inhibitor-NC (Figure 3A). Besides, miR-181a mimic increased cell proliferation in the EdU assay (Figure 3B), cell migration in transwell assay (Figure 3C), and the number of capillary-like network projections in the network formation assay (Figure 3D) of HUVECs relative to mimic-NC control. In contrast, miR-181a inhibitor treatment had the opposite results on these markers. In summary, overexpression of miR-181a augmented proliferation, migration, and capillary-like network formation in HUVECs *in vitro*.

miR-181a inhibits DACT2 and activates Yap-VEGF pathway by downregulating methylase MLL3 in HUVECs

The target genes of miR-181a in thyroid cancer were further analyzed by the online tools Targetscan, miDIP, RAID, StarBase, miRWalk, and miRDB. MLL3 (gene name KMT2C) was the only gene that was included in the intersection of the Venn diagram from these databases (Figure 4A). TargetScan revealed a potential binding site between miR-181a and MLL3 (Figure 4B). Luciferase reporter gene analysis revealed reduced luciferase activity in HEK293T cells co-transfected with Luc-MLL3-3′ UTR (wild-type) and miR-181a mimic but no such reduction in mutant Luc-MLL3-3′ UTR

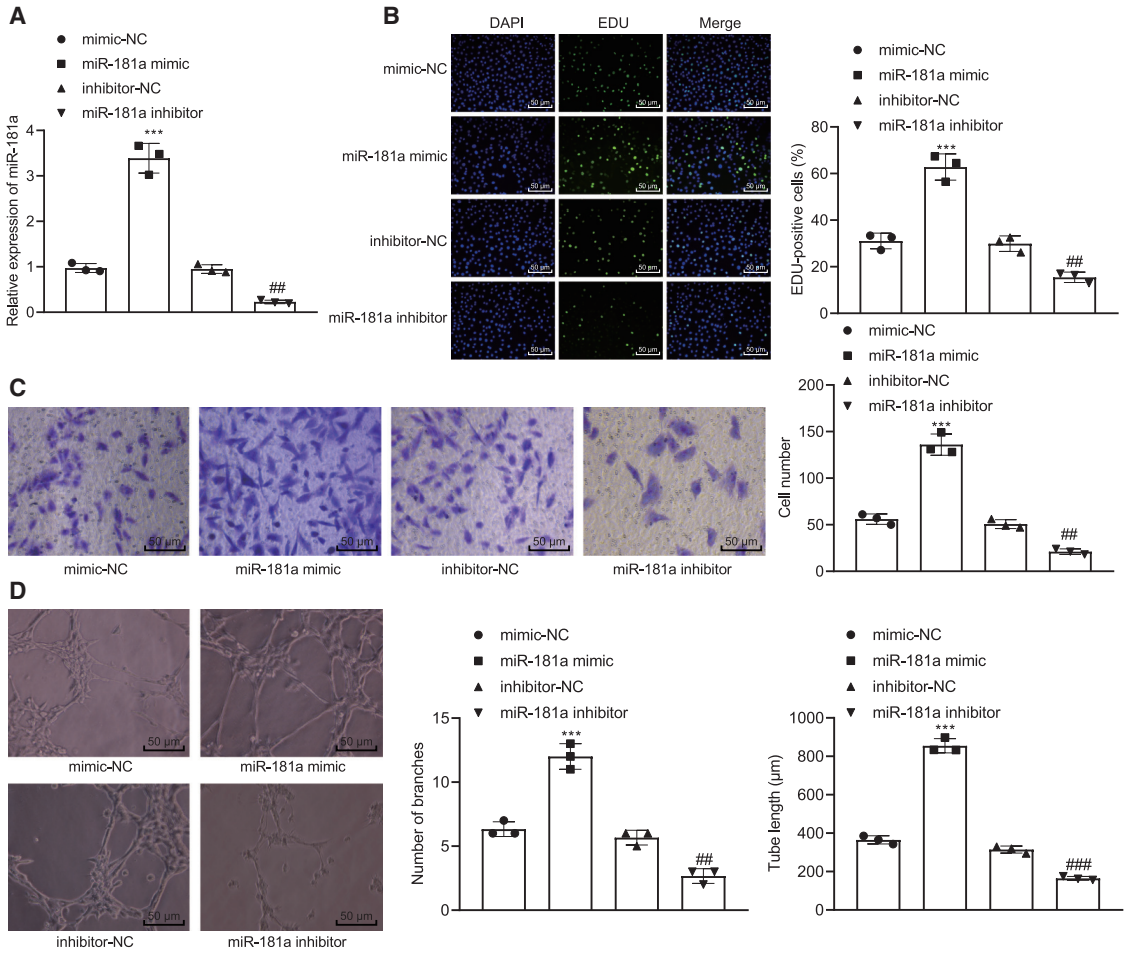

Figure 3. miR-181a inhibition reduces proliferation, migration, and capillary-like network formation in HUVECs

HUVECs were transfected with mimic-NC, miR-181a mimic, inhibitor-NC, or miR-181a inhibitor. (A) miR-181a expression analyzed by quantitative real-time PCR. (B) Cell proliferation tested by EdU assay (×200). (C) Cell migration determined by transwell assay (×200). (D) The formation of network-like structures by HUVECs (×200). *$p < 0.05$, **$p < 0.01$, ***$p < 0.001$ versus HUVECs transfected with mimic-NC; #$p < 0.05$, ##$p < 0.01$, ###$p < 0.001$ versus HUVECs transfected with inhibitor-NC. Data were presented as mean ± SD. One-way ANOVA with Tukey post hoc test was used to analyze data from multiple groups. The cell experiments were repeated in triplicate.

(Figure 4C). Moreover, miR-181a mimic reduced mRNA (Figure 4D) and protein (Figure 4E) expression of MLL3, while miR-181a inhibitor had the opposite effects in HUVECs. MLL3 can increase the activity in the enhancer region of DACT2, which then upregulates DACT2 expression.[18,19] Therefore, we next investigated whether MLL3 would increase DACT2 enhancer activity by catalyzing H3K4me1. After transfecting HUVECs with small interfering MLL3 (si-MLL3) or MLL3-vector control, the quantitative real-time PCR and western blot results illustrated that MLL3 silencing reduced MLL3, H3K4me1, and DACT2 mRNA (Figure 4F) and protein (Figure 4G) expression in HUVECs, whereas opposite effects occurred in the presence of oe-MLL3. In addition, the chromatin immunoprecipitation (ChIP) assay verified that MLL3 and H3K4me1 were significantly enriched in the DACT2 enhancer region (Figure 4H). We also found that miR-181a mimic diminished DACT2 mRNA (Figure 4I) and protein (Figure 4J) expression, while miR-181a inhibitor had the opposite effect. Furthermore, western blot results indicated that miR-181a mimic elevated YAP and VEGF expression but reduced the expression of phosphorylated YAP and H3K4me1 (Figure 4K), whereas miR-181a inhibitor had the opposite effect. Thus, miR-181a inhibited DACT2 and activated YAP-VEGF pathway by downregulating MLL3 expression in HUVECs.

Hypoxic PTC-secreted exosomal miR-181a promotes proliferation, migration, and angiogenesis of HUVECs

To determine whether hypoxic BCPAP cell-derived EXs affected HUVEC proliferation, migration, and angiogenesis *in vitro*, we treated HUVECs with PBS, normoxic-EXs, or hypoxia-EXs. Cell proliferation (Figure 5A), migration (Figure 5B), and capillary-like network formation (Figure 5C) of HUVECs were all enhanced by both normoxic-EXs and hypoxia-EXs, where the hypoxia-EX treatment

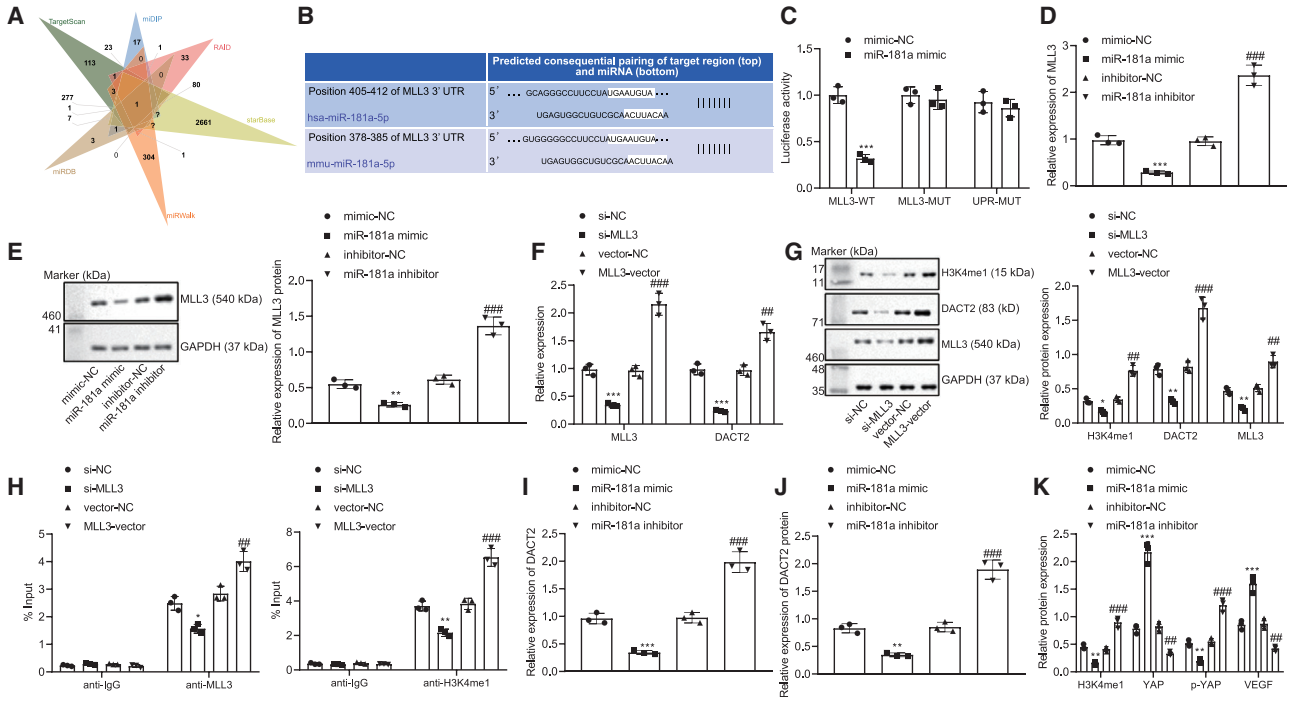

Figure 4. miR-181a inhibits DACT2 by downregulating methylase MLL3 to activate YAP-VEGF pathway in HUVECs

(A) Intersection of Venn diagram to show target genes of miR-181a-5p predicted by the online databases Targetscan, miDIP, RAID, StarBase, miRWalk, and miRDB. (B) The binding sites between miR-181a and MLL3 predicted via TargetScan. (C) Binding relationship between miR-181a and MLL3 determined by dual-luciferase reporter gene assay. (D) mRNA expression of MLL3 in HUVECs after corresponding miR-181a treatment analyzed by quantitative real-time PCR. (E) Protein expression of MLL3 in HUVECs after corresponding miR-181a treatment analyzed by western blot. (F) mRNA expression of MLL3 and DACT2 in HUVECs after alteration of MLL3 determined by quantitative real-time PCR. (G) Protein expression levels of MLL3, H3K4me1, and DACT2 in HUVECs after alteration of MLL3 determined by western blot. (H) MLL3 and H3K4me1 expression in DACT2 enhancer in HUVECs cells after alteration of MLL3 analyzed by ChIP assay. (I) mRNA expression of DACT2 in HUVECs after corresponding miR-181a treatment determined by quantitative real-time PCR. (J) Protein expression of DACT2 in HUVECs after corresponding miR-181a treatment analyzed by western blot. (K) Protein expression of H3K4me1, YAP, phosphorylated YAP, and VEGF in HUVECs after corresponding miR-181a treatment determined by western blot. *$p < 0.05$, **$p < 0.01$, ***$p < 0.001$ versus HUVECs transfected with mimic-NC or si-NC; #$p < 0.05$, ##$p < 0.01$, ###$p < 0.001$ versus HUVECs transfected with inhibitor-NC or vector-NC. Data were presented as mean ± SD. Unpaired t test was used to compare two sets of data. One-way ANOVA with Tukey post hoc test was used to analyze data from multiple groups. The cell experiments were repeated in triplicate.

caused stronger effects. In addition, enzyme-linked immunosorbent assay (ELISA) revealed that hypoxia-EXs increased VEGF concentration in the HUVEC culture medium (Figure 5D). Quantitative real-time PCR analysis showed that hypoxia-EXs reduced the mRNA levels of MLL3 and DACT2 in HUVECs (Figure 5E). Moreover, western blot data indicated that hypoxia-EXs downregulated the protein expression of MLL3, H3K4me1, DACT2, and phosphorylated YAP in HUVECs but upregulated YAP and VEGF expression (Figure 5F).

To further investigate the role of miR-181a in HUVECs angiogenesis, BCPAP cells were transfected with miR-181a inhibitor, followed by EX isolation. Quantitative real-time PCR illuminated that miR-181a inhibitor diminished miR-181a expression in BCPAP cells (Figure 5G) and hypoxia-induced EXs (Figure 5H). The cell proliferation (Figure 5I), migration (Figure 5J), and capillary-like network formation (Figure 5K) of HUVECs were reduced by hypoxia-EXs/miR-181a inhibitor. Thus, exosomal miR-181a could enhance proliferation, migration, and angiogenesis of HUVECs.

Hypoxic exosomal miR-181a promotes angiogenesis and tumor growth in nude mice

We next investigated the effect of hypoxia-induced exosomal miR-181a *in vivo*. Hypoxia-EXs increased angiogenesis around the chick chorioallantoic membrane (CAM; 5 mm), which illuminated the opposite effect in the presence of hypoxia-EXs/miR-181a inhibitor (Figure 6A). To investigate the effect of hypoxic exosomal miR-181a on tumorigenesis, we transplanted EX-treated BCPAP or K1 cells into nude mice. Hypoxia-EXs resulted in increased tumor mass (Figure 6B) and volume (Figure 6C), while hypoxia-EXs/miR-181a inhibitor showed the opposite trends. In addition, hypoxia-EXs increased VEGF levels in tumor tissues from nude mice, which was reversed by the treatment with hypoxia-EXs/miR-181a inhibitor (Figure 6D). Moreover, quantitative real-time PCR results revealed that miR-181a in tumor tissues was upregulated by hypoxia-EXs while downregulated by hypoxia-EXs/miR-181a inhibitor (Figure 6E). In contrast, hypoxia-EXs could decrease MLL3 expression in tumor tissues of nude mice, which was reversed by hypoxia-

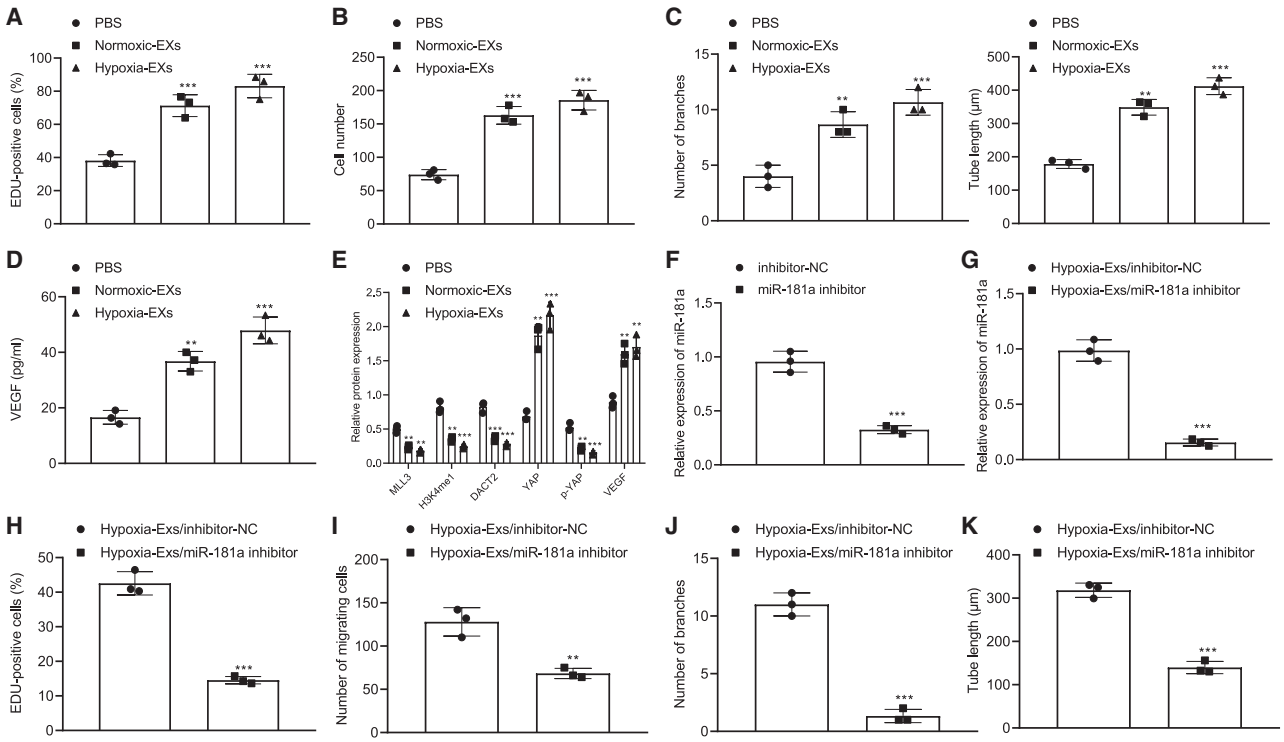

Figure 5. Exosomal miR-181a from hypoxia-treated PTC cells stimulates proliferation, migration, and angiogenesis in HUVECs

(A) HUVEC proliferation in the presence of PBS, normoxic-EXs, or hypoxia-EXs determined by EdU assay (×200). (B) HUVEC migration in the presence of PBS, normoxic-EXs, or hypoxia-EXs analyzed by transwell assay (×200). (C) The formation of network-like structures by HUVECs in the presence of PBS, normoxic-EXs, or hypoxia-EXs (×200). (D) VEGF concentration in culture medium in the presence of PBS, normoxic-EXs, or hypoxia-EXs determined by ELISA. (E) mRNA expression of MLL3 and DACT2 in HUVECs in the presence of PBS, normoxic-EXs, or hypoxia-EXs analyzed by quantitative real-time PCR. (F) Protein expression of MLL3, H3K4me1, DACT2, YAP, phosphorylated YAP, and VEGF of HUVECs in the presence of PBS, normoxic-EXs, or hypoxia-EXs analyzed by western blot. (G) miR-181a expression in BCPAP cells treated with miR-181a inhibitor detected by quantitative real-time PCR. (H) miR-181a expression in hypoxia-EXs/miR-181a inhibitor detected by quantitative real-time PCR. (I) HUVEC proliferation in the presence of hypoxia-EXs/miR-181a inhibitor tested by EdU assay (×200). (J) HUVEC migration in the presence of hypoxia-EXs/miR-181a inhibitor analyzed by transwell assay (×200). (K) The formation of network-like structures by HUVEC in the presence of hypoxia-EXs/miR-181a inhibitor (×200). *$p < 0.05$, **$p < 0.01$, ***$p < 0.001$ versus HUVEC treated with PBS or hypoxia-EXs/inhibitor-NC. Data were presented as mean ± SD. Unpaired t test was used to compare two sets of data. One-way ANOVA with Tukey post hoc test was used to compare data from multiple groups.

EXs/miR-181a inhibitor (Figure 6E). Furthermore, immunohistochemistry (IHC) data demonstrated that hypoxia-EXs increased the expression of VEGF (Figure 6F) and CD31-microvessel density (MVD; Figure 6G), whereas opposite effects were seen in the presence of hypoxia-EXs/miR-181a inhibitor. Taken together, hypoxic PTC-secreted exosomal miR-181a promoted angiogenesis and tumor growth in nude mice and downregulated MLL3 but upregulated VEGF and CD31 expression.

DISCUSSION

The incidence of PTC has increased in recent years, and patients with aggressive spread of this cancer resist therapy with VEGF receptor 2 (VEGFR2) inhibitor that normally attenuates angiogenesis in endothelial cells.[23] Emerging evidence has identified the regulatory effect of miRNAs on malignant phenotypes of tumor cells, which may present promising therapeutic targets in the treatment of PTC.[24] EXs can shuttle their cargos of proteins, mRNAs, and miRNAs between cells, and EXs secreted from cancer cells can have effects on the tumor microenvironment.[25] In the current study, the obtained findings revealed that exosomal miR-181a from hypoxia-induced PTC cells enhanced angiogenesis and tumor growth by downregulation of MLL3 and DACT2 and upregulation of YAP and VEGF signaling.

We uncovered in this study that miR-181a had oncogenic properties in PTC, which was consistent with results of a previous study[13] unveiling that miR-181a promoted thyroid cancer TPC-1 cell growth by inhibiting tumor suppressing RB1. The present results showed that miR-181a expression was increased in hypoxic PTC cells. A previous PTC-based bioinformatics analysis by Zhang et al.[26] has highlighted that miR-181a could modulate various differentially expressed genes in PTC to form a miRNA-mRNA regulatory network, a funding that helps substantially to broaden our understanding of the pathogenesis of PTC. In the present study, we also revealed that miR-181a overexpression induced HUVEC proliferation, migration, and angiogenesis. Certainly, angiogenesis plays an

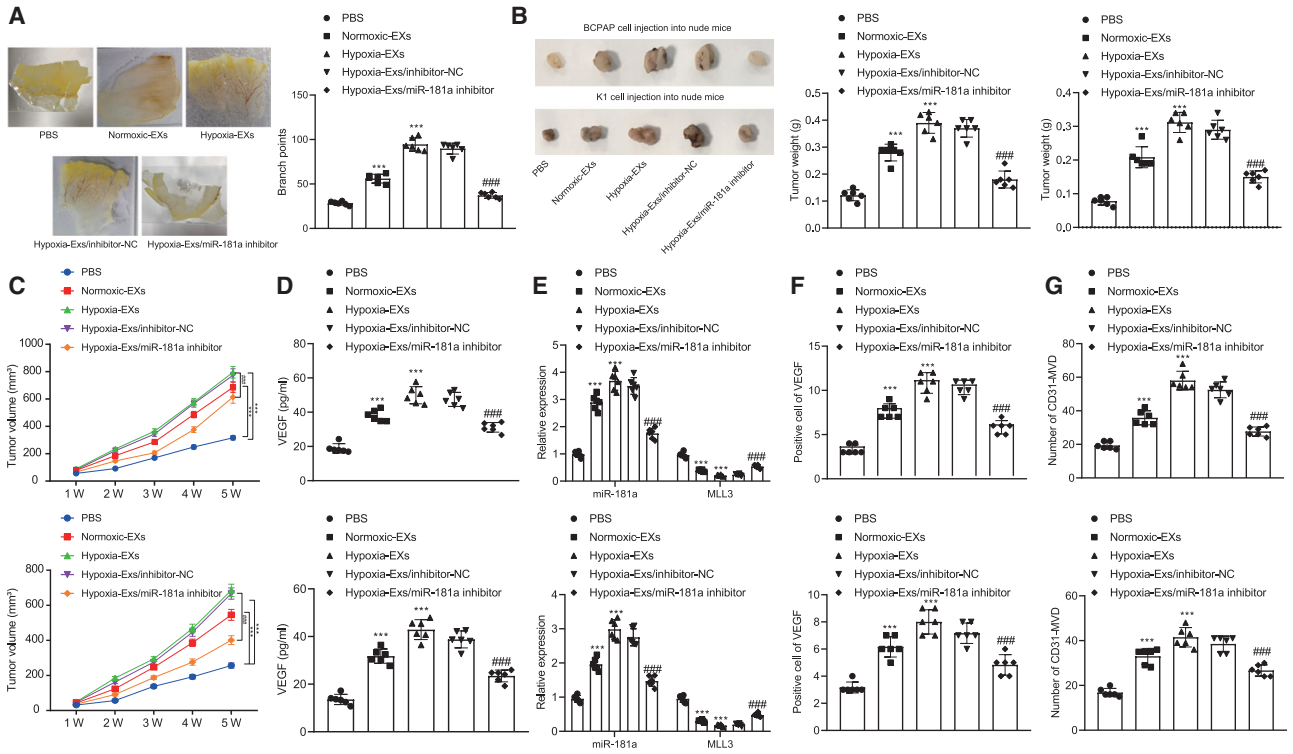

Figure 6. Exosomal miR-181a from hypoxic PTC cells induces angiogenesis and tumor growth in nude mice

CAM models were treated with PBS, normoxic-EXs, hypoxia-EXs, hypoxia-EXs/inhibitor-NC, or hypoxia-EXs/miR-181a inhibitor. (A) Angiogenesis analysis in CAM (5 mm) model. Nude mice were transplanted with BCPAP or K1 cells treated with PBS, normoxic-EXs, hypoxia-EXs, hypoxia-EXs/inhibitor-NC, or hypoxia-EXs/miR-181a inhibitor. (B) Tumor mass measurements. (C) Tumor volume measurements. (D) VEGF level in tumor tissues from nude mice. (E) mRNA expression of miR-181a and MLL3 detected by quantitative real-time PCR. (F) VEGF expression analyzed by IHC (×400). (G) CD31-MVD expression analyzed by IHC (×200). *$p < 0.05$, **$p < 0.01$, ***$p < 0.001$ versus CAM model or nude mice treated with PBS; #$p < 0.05$, ##$p < 0.01$, ###$p < 0.001$ versus CAM model or nude mice treated with hypoxia-EXs/inhibitor-NC. n = 6. Data were presented as mean ± SD. Unpaired t test was used to compare two sets of data. One-way ANOVA with Tukey post hoc test was used to analyze data from multiple groups. Data comparison between groups at different time points was performed by repeated-measures ANOVA, followed by Bonferroni post hoc test.

important role in cancer invasion and metastasis,[27] and growing evidence documents that miRNAs can accelerate cancer angiogenesis.[28,29] Intriguingly, angiogenic and metastatic effects of miR-181a have been suggested as factors in the mechanistic action of CXCR4 and RGS16 in chondrosarcoma.[30] Present findings add to this base of knowledge in suggesting a novel anti-angiogenic target and strategy for PTC treatment.

We further demonstrated that miR-181a can be delivered from PTC cells to HUVECs via PTC cell-derived EXs. EXs are extracellular vesicles serving as important factors for cell-to-cell communications.[31,32] Accumulating evidence suggests that EXs have a modulatory role in cancer progression.[33] More importantly, EXs accelerate angiogenesis through transportation of specific miRNAs. For example, exosomal miR-27a promoted angiogenesis in pancreatic cancer,[34] whereas another study elucidated high expression of PTC cell-derived exosomal miR-181a.[14] Furthermore, miR-181a inhibition reduced HUVEC cell proliferation, migration, and angiogenesis. Previous studies pointed out that miR-181a has been widely studied in a variety of human cancers. miR-181a can target the pro-apoptotic protein kinase C delta TBST gene to promote cancer cell resistance in cervical cancer.[11] In gastric cancer, miR-181a can target the tumor suppressor gene ATM.[12] For thyroid cancer, miR-181a can target the tumor suppressor RB1 to promote the growth of thyroid cancer cells.[13]

We next proceeded to probe the specific downstream mechanisms of miR-181a in thyroid cancer. miR-181a was found to target and inhibit MLL3, leading to the downregulation of DACT2. This decrease in DACT2 resulted in increased YAP-VEGF expression, which contributed to angiogenesis and tumorigenesis. Other lines of evidence document an association between MLL3 and cancer development.[15,16] A previous next-generation sequencing analysis on genes related to thyroid cancer identified mutations in the epigenetic regulator MLL3.[35] Through enhancing the enrichment of MLL3 and H3K4me3, an antitumor lncRNA SSTR5-AS1 could suppress the progression of laryngeal squamous cell carcinoma.[36] Previous molecular investigations have lined the development of thyroid cancer with an array of consistent abnormalities in pathways such as HIF1α-VEGF, which together orchestrate tumor growth and angiogenesis.[37] MLL3 acts as an H3K4me1

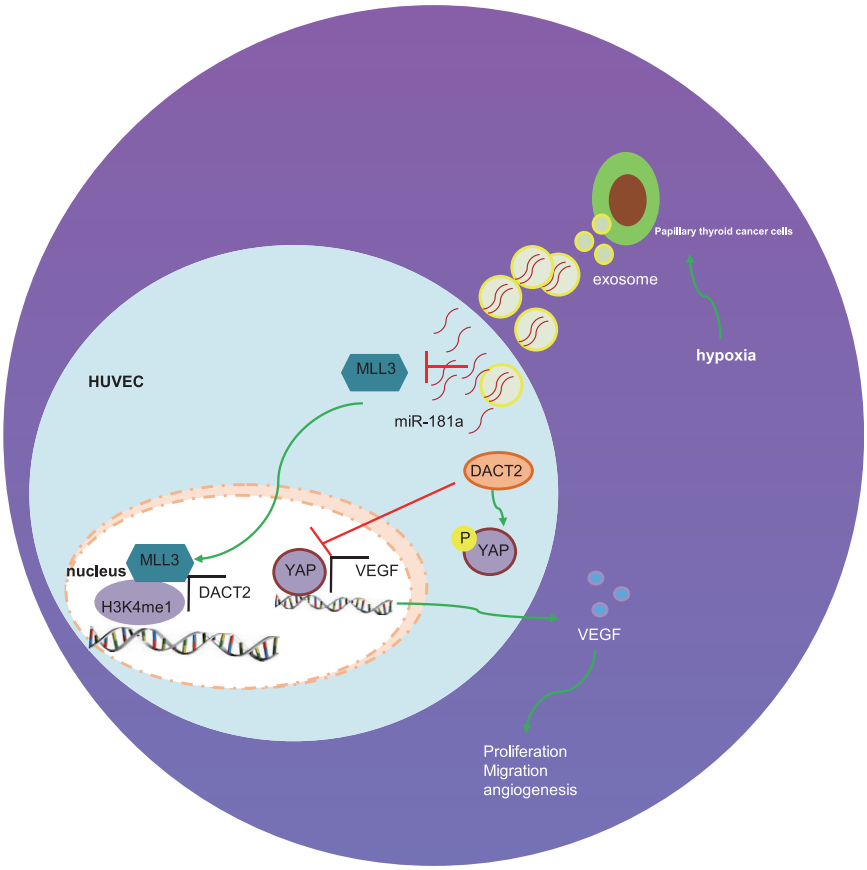

Figure 7. Mechanistic diagram showing effects of exosomal miR-181a from hypoxic PTC cells on PTC

Hypoxia promotes the release of miR-181a-loaded EXs from PTC cells. miR-181a is transported from PTC cells to HUVECs by EXs. miR-181a targets MLL3, leading to reduced H3K4me1 in the DACT2 enhancer region. Downregulation of DACT2 upregulates YAP, leading to the transcription of VEGF and angiogenesis.

methylase,[18] which could modulate the enhancer activity of DACT2 and the expression of DACT2.[18,19] In addition, we uncovered that inhibited expression of DACT2 resulted in the upregulation of YAP, which is consistent with the findings of a previous study in glioma.[38] Co-activation of YAP and VEGF has an important role in angiogenesis during the biological processes of cancers.[39,40] Results of our study support the notion that DACT2 downregulation increases the expression of YAP and VEGF, thus corroborating a previous study showing that YAP activated VEGF, which lead to angiogenesis.[41] Therefore, present results suggest that the YAP-VEGF pathway is significantly involved in thyroid tumor angiogenesis and growth. Our results also implied that miR-181a with the interplay of its downstream targets MLL3, DACT2, YAP, or VEGF may present a novel therapeutic target for the treatment of refractory PTC.

Conclusions

Present results indicate a new mechanism whereby miR-181a can modulate the angiogenesis of PTC, thus highlighting novel therapeutic targets for the treatment of PTC. We propose that new therapeutic strategies for PTC should be directed toward the ablation of hypoxic exosomal miR-181a, which may potentially be a clinically viable biomarker in treating PTC. miR-181a loaded in EXs derived from hypoxic PTCs promoted angiogenesis and tumor growth through a pathway involving downregulation of DACT2, MLL3, and activation of YAP-VEGF signaling pathway (Figure 7). However, results from this study require generalization by confirming the pro-angiogenic effects of hypoxic exosomal miR-181a on the diverse other types of PTC cell lines. Moreover, the values of these findings may be limited by the lack of a series of rescue assays to demonstrate the link of miR-181a, MLL3, and the YAP-VEGF signaling pathway, which should be further performed in future studies.

MATERIALS AND METHODS

Ethics statement

All animal experiment protocols involved in this study were performed in strict accordance with the Guide for the Care and Use of Laboratory Animals and were approved by the Institutional Research Ethics Committee of Sun Yat-sen University Cancer Center. Efforts were taken to minimize discomfort and numbers of animals.

Bioinformatics analysis of genes involved in thyroid cancer

Thyroid cancer-related miRNA expression datasets Gene Expression Omnibus (GEO): GSE73182 and GSE103996 were downloaded from the GEO database (https://www.ncbi.nlm.nih.gov/gds). GEO: GSE73182 includes 24 samples, including 5 control and 19 thyroid cancer samples. There were 34 samples in GEO: GSE103996, including 6 control and 28 thyroid cancer samples. The "limma" package (http://www.bioconductor.org/packages/release/bioc/html/limma.html) in R was utilized for differential analysis of gene expression in GEO: GSE73182 ($|\log FC| > 1$, $p < 0.01$) and GSE103996 ($|\log FC| > 1$, $p < 0.01$). The differential expression of these miRNAs was validated by the StarBase analysis (http://starbase.sysu.edu.cn/). Further, target genes of the key miRNA were predicted by Targetscan (cumulative weighted context++ score > 0.1; http://www.targetscan.org/vert_71/), miDIP (integrated score > 0.65; http://ophid.utoronto.ca/mirDIP/), RAID (score > 0.65; http://www.rna-society.org/raid2/index.html), StarBase, miRWalk (energy < −24.0; http://mirwalk.umm.uni-heidelberg.de/), and miRDB (Target Score > 95; http://www.mirdb.org/). Key genes of these databases were

intersected by the Venn diagram. After determining the most important genes in the intersection, we used a literature search to find their downstream pathways.

Cell culture

Human PTC cell lines BCPAP (BeNa Culture Collection, Beijing, China) and K1 (Sigma-Aldrich, St. Louis, MO, USA) were cultured in RPMI 1640 (GIBCO, Carlsbad, CA, USA) and Dulbecco's modified Eagle medium (DMEM), respectively. Both media were supplemented with 10% fetal bovine serum (FBS; Atlanta Biologicals, Flowery Branch, GA, USA), penicillin (10,000 IU/mL), streptomycin (10,000 μg/mL; MediaTech, Laval, QC, Canada), and 2 mM *L*-glutamine (MediaTech). Human normal thyroid cell HTori-3 (DMSZ, Braunschweig, Germany) was cultured in DMEM.[42]

HUVECs (Institute of Cell Biology of the Chinese Academy of Sciences, Shanghai, China) were cultured in MCDB 131 medium (GIBCO) supplemented with 5% microvascular growth supplement (GIBCO) and 1% Gluta MAX (GIBCO), followed by incubation in a humidified incubator at 37°C with 5% CO_2.[22]

Isolation and identification of EXs from BCPAP cells

EX-depleted FBS was obtained by overnight ultracentrifugation at 120,000 × *g* at 4°C, followed by filtration through 0.22-μm filters. BCPAP cells were cultured in DMEM as noted above to 80%–90% confluence, and then replaced with RPMI 1640 medium containing 10% EX-depleted FBS and incubated under normoxic (20% O_2) or hypoxic (1% O_2) conditions for 12 h. Next cell culture media were then harvested and centrifuged at 300 × *g* for 10 min, at 2,000 × *g* for 10 min, and at 10,000 × *g* (Beckman Coulter, Brea, CA, USA) for 30 min to remove cell debris. The pellet was resuspended for another ultracentrifugation at 100,000 × *g* for 70 min and finally formulated in 50–100 μL phosphate buffered saline (PBS). EXs were isolated by the ExoQuick reagent (System Biosciences, Palo Alto, CA, USA). In brief, the resuspended pellet was incubated with ExoQuick reagent at ratio of 5:1 for 12 h, and then centrifuged at 1,500 × *g* for 30 min. Precipitated EXs were resuspended in 100 μL PBS and stored at −80°C for further experiments.[43]

A Delsa Nano Analyzer (Beckman Coulter, Brea, CA, USA) was applied to determine the size distribution of EXs. Capture and analysis settings were manually adjusted according to the manufacturer's instructions. In addition, EXs were fixed in 4% glutaraldehyde, placed on carbon-coated copper grids, and stained with 2% uranyl acetate for examination by transmission electron microscopy (TEM; JEM-1010, JEOL, Tokyo, Japan).[44]

EX uptake

EXs (20 μg) were labeled with PKH67 green fluorescent dye (Sigma-Aldrich) based on the manufacturer's instructions. Labeled exosomal particles were resuspended and added to unstained HUVEC cells for exosomal uptake experiments. After incubating for 12 h at 37°C, cells were visualized with a confocal microscope (Zeiss Meta 510, Thornwood, NY, USA).[43]

miR-181a delivery

BCPAP cells were cultured and transfected in transwell chambers (pore size: 0.4 mm, Thermo Fisher Scientific, Waltham, MA, USA) with 10 nM green fluorescent 3′ FAM labeled miR-181a oligo (GeneCore Biotechnology, Shanghai, China) for 24 h. HUVECs at the bottom side of the transwell were co-cultured with BCPAP cells for 24 h. HUVEC cells were fixed with 4% paraformaldehyde and visualized under a laser scanning confocal microscope (LSCM).[45]

Transfection in BCPAP And HUVECs

BCPAP cells or HUVECs were transfected with miR-181a mimic (100 pmol), miR-181a inhibitor or their corresponding negative controls (NCs; RiboBio, Guangzhou, China) by Lipofectamine 2000 according to the manufacturer's instructions (Invitrogen, Carlsbad, CA, USA). In addition, HUVECs were also transfected with si-NC, si-MLL3, vector-NC, and MLL3-vector (Gene Pharma, Shanghai, China) by Lipofectamine 2000 (Invitrogen).[46]

Quantitative real-time PCR

Total RNA was extracted from cells and EXs using Trizol reagent (Invitrogen). cDNA was synthesized using a reverse transcription kit (RR047A, Takara, Tokyo, Japan). miRNA was reverse transcribed by miRNA First Strand cDNA Synthesis (Tailing Reaction) kit (B532451-0020, Sangon, Shanghai, China). cDNA was subjected to qPCR using a SYBR Premix Ex Taq II (Perfect Real Time) kit (DRR081, Takara, Japan) in a real-time PCR machine (ABI 7500, ABI, Foster City, CA, USA). miRNA expression level was normalized to the internal control U6, while mRNA expression level was normalized to glyceraldehyde-3-phosphate dehydrogenase (GAPDH). Relative expression of target gene was calculated by the $2^{-\Delta\Delta CT}$ method. In addition, cel-miR-39 was used for normalization of EXs (primers were purchased from RIBO, Guangzhou, China). miRNA negative primer and U6 forward primer were provided by the miRNA First Strand cDNA Synthesis (Tailing Reaction) kit, and other primers were synthetized by Sangon (Table S1).[47–49]

Western blot assay

Cells or EXs were lysed using radioimmunoprecipitation assay (RIPA) lysis buffer containing complete protease and phosphatase inhibitor (Sigma-Aldrich). 30 μg of protein from each sample was loaded and separated on sodium dodecyl sulfate polyacrylamide gel electrophoresis gel (SDS-PAGE), which was transferred to a 0.22-μm polyvinylidene fluoride membrane (PVDF; Millipore, Burlington, MA, USA). The membrane was blocked with 5% skim milk and incubated with primary antibodies: mouse anti-CD9 (1:500, sc-13118, Santa Cruz, CA, USA), mouse anti-CD81 (1:500, sc-7637, Santa Cruz), mouse anti-tumor susceptibility gene101 (TSG101; 1:500, sc-7964, Santa Cruz), mouse anti-heat shock protein 70 (HSP70; 1:500, sc-32239, Santa Cruz), mouse anti-ALIX (1:500, sc-53540, Santa Cruz), mouse anti-flotillin-1 (1:500, sc-74566, Santa Cruz), mouse anti-VEGF (1:100, sc-7269, Santa Cruz), rabbit anti-MLL3 (1:1,000, ABE1851, Sigma), rabbit anti-DACT2 (1:1,000, ab79042, Abcam, Cambridge, MA, USA), rabbit anti-phosphorylated YAP (1:1,000, ab62751, Abcam), rabbit anti-YAP (1:1,000, ab81183,

Abcam), rabbit anti-H3K4me1 (1:500, ab8895, Abcam), and rabbit anti-GAPDH (1:2,500, ab9485, Abcam) overnight at 4°C. The next day, the membrane was washed with TRIS-buffered saline with 0.5% Tween 20 and incubated with horseradish peroxidase-conjugated secondary antibody (immunoglobulin G [IgG]; 1:20,000, ab205718, ab205719, Abcam) at room temperature and then washed with TBST. Membranes were developed by Thermo Pierce chemiluminescent (ECL) western blot substrate (Thermo Fisher Scientific) using a Tanon 5200 system (Tanon, Shanghai, China).[50]

Dual-luciferase reporter gene assay

Wild-type or mutant MLL3 3′ UTR-psiCHECK-2 plasmid (Promega) were co-transfected with miR-181a mimic or mimic-NC into 293T cells using Lipofectamine 2000 reagent (Invitrogen). Lysates were harvested 48 h after transfection. Firefly luciferase intensity was measured and normalized to Renilla luciferase intensity using a dual-luciferase reporter kit (Promega Corporation, Madison, WI, USA).

ChIP assay

ChIP experimental protocol was performed as previously described.[48,51] In brief, cell lysate was sonicated and then immunoprecipitated overnight using MLL3, H3K4me1 (2 μg for 25 μg of chromatin, ab8895) or non-specific IgG (1:1,000, ab171870, Abcam) antibodies as control. The next day samples were incubated with protein beads to form the protein-antibody-bead complex. After stringent washing, immunoprecipitated DNA was isolated used for qPCR. Anti-MLL3 was generated against the aa 443-590 (α-MLL3-NTD) or aa 2951-3091 (α-MLL3-MR) protein. The primers of the enhancer region of DACT2 were shown as follows: forward: 5′-ACAGGACTGGCTAAACGCAA-3′ and reverse: 5′-AGGTGCAAATGCTGCCCTAT-3′.[18]

Cell counting kit-8 (CCK-8) assay

The CCK-8 kit (C0037, Beyotime Institute of Biotechnology, Shanghai, China) was used for the measurement of cell viability. Cells were cultured in a 96-well plate at a density of 2×10^3 cells/well for 24 h. Following 24-h transfection, 10 μL CCK-8 reagents were added into 100 μL complete medium and the cells were cultured for 24, 48, or 72 h. Absorbance was measured using Multiskan FC microplate reader (51119100, Thermo Fisher Scientific) at the respective time points.

5-ethynyl-2′-erdeoxyuridine (EDU) assay

HUVECs in logarithmic growth phase were co-cultured with EXs and seeded into 96-well plates (3×10^4 cells/well). Cells were incubated with 100 μL of EdU medium for 2 h and then incubated with 100 μL fixative for 30 min, followed by 5-min incubation with 2 mg/mL glycine. Cells were incubated with 100 μL PBS containing 0.5% Triton X-100 for 10 min, stained with 1× Apollo for 30 min and 100 μL of 1 × Hoechst 33342 reaction solution for 30 min in the dark. Anti-fluorescent quencher (100 μL) was added to each well. A total of 6–10 fields were randomly selected per well for visualization and imaging under a fluorescence microscope.

Transwell assay

HUVECs in logarithmic growth phase co-cultured with EXs were added on the upper transwell at a density of 1×10^4 cells/μL, whereas FBS (800 μL, 20%) was added to the lower transwell chamber. Cells were incubated at 37°C for 24 h, whereupon cells were fixed with 5% paraformaldehyde for 10 min and then stained with 0.1% crystal violet for 30 min. Cells on the surface were wiped away by cotton swabs for observation, imaging, and quantification under an inverted microscope.

Network formation assay

Calpain-labeled HUVECs were seeded into a 24-well plate at a density of 2×10^5 cells/mL. Adherent cells were incubated with 5% CO_2 at 37°C for 12 h. The capillary-like network projections (number and length) were analyzed under a confocal microscope.

Determination of angiogenesis in chicken Cam

60 chicken embryos were incubated at 37.5°C ± 0.5°C under 65% humidity for 3 days. The growth of the vascular network was detected by the candlelight method. A total of 48 well-developed vascular networks were obtained. HUVECs were treated with PBS, normoxic BCPAP cell-derived EXs (normoxic-EXs), EXs from hypoxia BCPAP cells (hypoxia-EXs), EXs from hypoxia BCPAP cells transfected with inhibitor-NC (hypoxia-EXs/inhibitor-NC), or EXs from hypoxia BCPAP cells transfected with miR-181a inhibitor (hypoxia-EXs/miR-181a inhibitor), respectively, and then injected into chicken embryos (12 embryos/group). Fertilized chicken embryos were sterilized with ethanol on day 7 of incubation. A small window (1.5 cm × 1.5 cm) was created in the egg and a filter paper was fixed with tape on the CAM and yolk sac membrane with relatively few blood vessels. After a 10-day further incubation in the incubator, the tape covering the chicken embryos was removed and angiogenesis was observed under a microscope and imaged with a digital camera.

ELISA

The concentration of VEGF in HUVEC cell culture supernatant was measured by an ELISA kit (69-50, 049, MSK Biotechnology, Wuhan, China). Absorbance was detected at 450 nm by a microplate reader (Synergy 2, BioTek, Winooski, VT, USA) within 3 min.

For transplanted tumor, 50 mg of tissue was added to 4–5 mL of 0.86% PBS, homogenized for 2 min, and centrifuged at 1,610 × *g* for 10 min at 4°C to obtain tissue supernatant. VEGF concentration in the supernatant was measured by the ELSA kit (69-50, 049, MSK Biotechnology). Absorbance was detected at 450 nm by a microplate reader (Synergy 2, BioTek).[52]

Tumor xenografts in nude mice

Female BALB/C nude mice (n = 60, 3–4 weeks old, 15–19 g, Slac-Jingda Animal Laboratory, Hunan, China) were randomly divided into ten groups (five groups for BCPAP cell line and five for K1 cell line, n = 6 per group): BCPAP cells or K1 cells were treated with PBS, normoxic-EXs, hypoxia-EXs, hypoxia-EXs/inhibitor-NC, or hypoxia-EXs/miR-181a inhibitor. Single cell suspension (4×10^6

cells/mL) was injected subcutaneously into the back of nude mice using a disposable sterile syringe. Tumor volume was calculated as $V = W^2 \times L \times 0.5$, where W is the width and L is the length of the tumor. After 35 days, nude mice were euthanized. Implanted tumors were resected and immersion-fixed in 4% neutral formaldehyde overnight. Tissues were then embedded in paraffin and sectioned to a thickness of 5 μm.

IHC

IHC was performed using the streptavidin-biotin-peroxidase complex method. In brief, tumor tissues were fixed, paraffin-embedded, dewaxed, and rehydrated, followed by antigen retrieval. Tissues were then incubated with VEGF antibody (1:100, ab72807, Abcam) at 4°C overnight. The next day, tissues were incubated in biotinylated secondary antibody for 30 min at 37°C. Tissues were developed with diaminobenzidine (DAB) solution, followed by hematoxylin counterstaining and imaging under an optical microscope.

MVD assay was analyzed by streptavidin peroxidase immunohistochemical staining with primary CD31 antibody (1:50, ab28364, Abcam). 100 cells in each of five randomly selected regions were counted under the microscope. MVD was presented as the percentage of $CD31^+$ cells.

Statistical analysis

Data analysis was performed by SPSS version 21.0 (IBM, Armonk, NY, USA). Data were presented as mean ± standard deviation (SD). The unpaired t test was utilized to compare unpaired data between two groups. One-way analysis of variance (ANOVA) with Tukey post hoc test was applied to compare data from multiple groups. Tumor volumes between groups at different time points were performed by repeated-measures ANOVA, followed by Bonferroni post hoc test. The comparison of optical density (OD) values reflecting cell viability at different time points was performed by two-way ANOVA. $p < 0.05$ indicated statistically significant difference.

SUPPLEMENTAL INFORMATION

Supplemental information can be found online at https://doi.org/10.1016/j.omtn.2021.02.027.

ACKNOWLEDGMENTS

We acknowledge and appreciate our colleagues for their valuable efforts and comments on this paper. This study was supported by the National Natural Science Foundation of China (grant no. 81402213) and the Characteristic Innovation Projects of General Colleges and Universities in Guangdong Province (grant no. 2019KTSCX009) award to Y.W., and the National Natural Science Foundation of China (grant no. 81874220) and the Guangdong Basic and Applied Basic Research Foundation (grant no. 2020A151501030) award to L.Z.

AUTHOR CONTRIBUTIONS

Y.W. conceived and designed the research. A.C. performed the experiments. Y.Y. interpreted the results of the experiments. H.Y. analyzed the data. J.L. prepared the figures. S.L. drafted the paper. L.Z. edited and revised the manuscript. All authors read and approved the final version of the manuscript.

DECLARATION OF INTERESTS

The authors declare no competing interests.

REFERENCES

1. Roman, B.R., Morris, L.G., and Davies, L. (2017). The thyroid cancer epidemic, 2017 perspective. Curr. Opin. Endocrinol. Diabetes Obes. *24*, 332–336.
2. Yapa, S., Mulla, O., Green, V., England, J., and Greenman, J. (2017). The Role of Chemokines in Thyroid Carcinoma. Thyroid *27*, 1347–1359.
3. Fallahi, P., Mazzi, V., Vita, R., Ferrari, S.M., Materazzi, G., Galleri, D., Benvenga, S., Miccoli, P., and Antonelli, A. (2015). New therapies for dedifferentiated papillary thyroid cancer. Int. J. Mol. Sci. *16*, 6153–6182.
4. Kojic, K.L., Kojic, S.L., and Wiseman, S.M. (2012). Differentiated thyroid cancers: a comprehensive review of novel targeted therapies. Expert Rev. Anticancer Ther. *12*, 345–357.
5. Wu, F., Li, F., Lin, X., Xu, F., Cui, R.R., Zhong, J.Y., Zhu, T., Shan, S.K., Liao, X.B., Yuan, L.Q., and Mo, Z.H. (2019). Exosomes increased angiogenesis in papillary thyroid cancer microenvironment. Endocr. Relat. Cancer *26*, 525–538.
6. Xu, Z.H., Miao, Z.W., Jiang, Q.Z., Gan, D.X., Wei, X.G., Xue, X.Z., Li, J.Q., Zheng, F., Qin, X.X., Fang, W.G., et al. (2019). Brain microvascular endothelial cell exosome-mediated S100A16 up-regulation confers small-cell lung cancer cell survival in brain. FASEB J. *33*, 1742–1757.
7. Withrow, J., Murphy, C., Liu, Y., Hunter, M., Fulzele, S., and Hamrick, M.W. (2016). Extracellular vesicles in the pathogenesis of rheumatoid arthritis and osteoarthritis. Arthritis Res. Ther. *18*, 286.
8. Di Gregoli, K., Jenkins, N., Salter, R., White, S., Newby, A.C., and Johnson, J.L. (2014). MicroRNA-24 regulates macrophage behavior and retards atherosclerosis. Arterioscler. Thromb. Vasc. Biol. *34*, 1990–2000.
9. Wang, J., Wu, L., Jin, Y., Li, S., and Liu, X. (2020). Identification of key miRNAs in papillary thyroid carcinoma based on data mining and bioinformatics methods. Biomed. Rep. *12*, 11–16.
10. Niu, J., Xue, A., Chi, Y., Xue, J., Wang, W., Zhao, Z., Fan, M., Yang, C.H., Shao, Z.M., Pfeffer, L.M., et al. (2016). Induction of miRNA-181a by genotoxic treatments promotes chemotherapeutic resistance and metastasis in breast cancer. Oncogene *35*, 1302–1313.
11. Ke, G., Liang, L., Yang, J.M., Huang, X., Han, D., Huang, S., Zhao, Y., Zha, R., He, X., and Wu, X. (2013). MiR-181a confers resistance of cervical cancer to radiation therapy through targeting the pro-apoptotic PRKCD gene. Oncogene *32*, 3019–3027.
12. Zhang, X., Nie, Y., Li, X., Wu, G., Huang, Q., Cao, J., Du, Y., Li, J., Deng, R., Huang, D., et al. (2014). MicroRNA-181a functions as an oncomir in gastric cancer by targeting the tumour suppressor gene ATM. Pathol. Oncol. Res. *20*, 381–389.
13. Le, F., Luo, P., Yang, Q.O., and Zhong, X.M. (2017). MiR-181a promotes growth of thyroid cancer cells by targeting tumor suppressor RB1. Eur. Rev. Med. Pharmacol. Sci. *21*, 5638–5647.
14. Samsonov, R., Burdakov, V., Shtam, T., Radzhabova, Z., Vasilyev, D., Tsyrlina, E., Titov, S., Ivanov, M., Berstein, L., Filatov, M., et al. (2016). Plasma exosomal miR-21 and miR-181a differentiates follicular from papillary thyroid cancer. Tumour Biol. *37*, 12011–12021.
15. Chen, D., Gong, L., Jiang, Q., Wang, X., and Zhang, B. (2016). Interaction between MLL3 genetic polymorphisms, smoking, and alcohol drinking in laryngeal cancer: a case-control study. Cancer Med. *5*, 527–533.
16. Li, B., Liu, H.Y., Guo, S.H., Sun, P., Gong, F.M., and Jia, B.Q. (2014). Association of MLL3 expression with prognosis in gastric cancer. Genet. Mol. Res. *13*, 7513–7518.
17. Sze, C.C., and Shilatifard, A. (2016). MLL3/MLL4/COMPASS Family on Epigenetic Regulation of Enhancer Function and Cancer. Cold Spring Harb. Perspect. Med. *6*, a026427.
18. Wang, L., Zhao, Z., Ozark, P.A., Fantini, D., Marshall, S.A., Rendleman, E.J., Cozzolino, K.A., Louis, N., He, X., Morgan, M.A., et al. (2018). Resetting the

epigenetic balance of Polycomb and COMPASS function at enhancers for cancer therapy. Nat. Med. *24*, 758–769.

19. Zhao, Z., Herman, J.G., Brock, M.V., Sheng, J., Zhang, M., Liu, B., and Guo, M. (2014). Methylation of DACT2 promotes papillary thyroid cancer metastasis by activating Wnt signaling. PLoS ONE *9*, e112336.
20. Zhu, C.C., Chen, C., Xu, Z.Q., Zhao, J.K., Ou, B.C., Sun, J., Zheng, M.H., Zong, Y.P., and Lu, A.G. (2018). CCR6 promotes tumor angiogenesis via the AKT/NF-κB/VEGF pathway in colorectal cancer. Biochim. Biophys. Acta Mol. Basis Dis. *1864*, 387–397.
21. Kim, T.K., Park, C.S., Jang, J., Kim, M.R., Na, H.J., Lee, K., Kim, H.J., Heo, K., Yoo, B.C., Kim, Y.M., et al. (2018). Inhibition of VEGF-dependent angiogenesis and tumor angiogenesis by an optimized antibody targeting CLEC14a. Mol. Oncol. *12*, 356–372.
22. Sun, W., Wang, X., Li, J., You, C., Lu, P., Feng, H., Kong, Y., Zhang, H., Liu, Y., Jiao, R., et al. (2018). MicroRNA-181a promotes angiogenesis in colorectal cancer by targeting SRCIN1 to promote the SRC/VEGF signaling pathway. Cell Death Dis. *9*, 438.
23. Shaik, S., Nucera, C., Inuzuka, H., Gao, D., Garnaas, M., Frechette, G., Harris, L., Wan, L., Fukushima, H., Husain, A., et al. (2012). SCF(β-TRCP) suppresses angiogenesis and thyroid cancer cell migration by promoting ubiquitination and destruction of VEGF receptor 2. J. Exp. Med. *209*, 1289–1307.
24. Boos, L.A., Schmitt, A., Moch, H., Komminoth, P., Simillion, C., Marinoni, I., Nikiforov, Y.E., Nikiforova, M.N., Perren, A., and Dettmer, M.S. (2019). MiRNAs Are Involved in Tall Cell Morphology in Papillary Thyroid Carcinoma. Cancers (Basel) *11*, 885.
25. Ohzawa, H., Saito, A., Kumagai, Y., Kimura, Y., Yamaguchi, H., Hosoya, Y., Lefor, A.K., Sata, N., and Kitayama, J. (2020). Reduced expression of exosomal miR-29s in peritoneal fluid is a useful predictor of peritoneal recurrence after curative resection of gastric cancer with serosal involvement. Oncol. Rep. *43*, 1081–1088.
26. Zhang, C., Bo, C., Guo, L., Yu, P., Miao, S., and Gu, X. (2019). BCL2 and hsa-miR-181a-5p are potential biomarkers associated with papillary thyroid cancer based on bioinformatics analysis. World J. Surg. Oncol. *17*, 221.
27. Saharinen, P., Eklund, L., Pulkki, K., Bono, P., and Alitalo, K. (2011). VEGF and angiopoietin signaling in tumor angiogenesis and metastasis. Trends Mol. Med. *17*, 347–362.
28. Lu, Y., Qin, T., Li, J., Wang, L., Zhang, Q., Jiang, Z., and Mao, J. (2017). MicroRNA-140-5p inhibits invasion and angiogenesis through targeting VEGF-A in breast cancer. Cancer Gene Ther. *24*, 386–392.
29. Tiwari, A., Mukherjee, B., and Dixit, M. (2018). MicroRNA Key to Angiogenesis Regulation: MiRNA Biology and Therapy. Curr. Cancer Drug Targets *18*, 266–277.
30. Sun, X., Charbonneau, C., Wei, L., Chen, Q., and Terek, R.M. (2015). miR-181a Targets RGS16 to Promote Chondrosarcoma Growth, Angiogenesis, and Metastasis. Mol. Cancer Res. *13*, 1347–1357.
31. Mathieu, M., Martin-Jaular, L., Lavieu, G., and Théry, C. (2019). Specificities of secretion and uptake of exosomes and other extracellular vesicles for cell-to-cell communication. Nat. Cell Biol. *21*, 9–17.
32. Bang, C., and Thum, T. (2012). Exosomes: new players in cell-cell communication. Int. J. Biochem. Cell Biol. *44*, 2060–2064.
33. Maia, J., Caja, S., Strano Moraes, M.C., Couto, N., and Costa-Silva, B. (2018). Exosome-Based Cell-Cell Communication in the Tumor Microenvironment. Front. Cell Dev. Biol. *6*, 18.
34. Shang, D., Xie, C., Hu, J., Tan, J., Yuan, Y., Liu, Z., and Yang, Z. (2020). Pancreatic cancer cell-derived exosomal microRNA-27a promotes angiogenesis of human microvascular endothelial cells in pancreatic cancer via BTG2. J. Cell. Mol. Med. *24*, 588–604.
35. Landa, I., Ibrahimpasic, T., Boucai, L., Sinha, R., Knauf, J.A., Shah, R.H., Dogan, S., Ricarte-Filho, J.C., Krishnamoorthy, G.P., Xu, B., et al. (2016). Genomic and transcriptomic hallmarks of poorly differentiated and anaplastic thyroid cancers. J. Clin. Invest. *126*, 1052–1066.
36. Wang, B., Zhao, L., Chi, W., Cao, H., Cui, W., and Meng, W. (2019). Aberrant methylation-mediated downregulation of lncRNA SSTR5-AS1 promotes progression and metastasis of laryngeal squamous cell carcinoma. Epigenetics Chromatin *12*, 35.
37. Lv, Y., Sun, Y., Shi, T., Shi, C., Qin, H., and Li, Z. (2016). Pigment epithelium-derived factor has a role in the progression of papillary thyroid carcinoma by affecting the HIF1α-VEGF signaling pathway. Oncol. Lett. *12*, 5217–5222.
38. Tan, Y., Li, Q.M., Huang, N., Cheng, S., Zhao, G.J., Chen, H., Chen, S., Tang, Z.H., Zhang, W.Q., Huang, Q., and Cheng, Y. (2017). Upregulation of DACT2 suppresses proliferation and enhances apoptosis of glioma cell via inactivation of YAP signaling pathway. Cell Death Dis. *8*, e2981.
39. Elaimy, A.L., and Mercurio, A.M. (2018). Convergence of VEGF and YAP/TAZ signaling: Implications for angiogenesis and cancer biology. Sci. Signal. *11*, eaau1165.
40. Wang, X., Freire Valls, A., Schermann, G., Shen, Y., Moya, I.M., Castro, L., Urban, S., Solecki, G.M., Winkler, F., Riedemann, L., et al. (2017). YAP/TAZ Orchestrate VEGF Signaling during Developmental Angiogenesis. Dev. Cell *42*, 462–478.e7.
41. Zhu, M., Liu, X., Wang, Y., Chen, L., Wang, L., Qin, X., Xu, J., Li, L., Tu, Y., Zhou, T., et al. (2018). YAP via interacting with STAT3 regulates VEGF-induced angiogenesis in human retinal microvascular endothelial cells. Exp. Cell Res. *373*, 155–163.
42. Kamat, A., Rajoria, S., George, A., Suriano, R., Shanmugam, A., Megwalu, U., Prakash, P.B., Tiwari, R., and Schantz, S. (2011). Estrogen-mediated angiogenesis in thyroid tumor microenvironment is mediated through VEGF signaling pathways. Arch. Otolaryngol. Head Neck Surg. *137*, 1146–1153.
43. Wang, X., Luo, G., Zhang, K., Cao, J., Huang, C., Jiang, T., Liu, B., Su, L., and Qiu, Z. (2018). Hypoxic Tumor-Derived Exosomal miR-301a Mediates M2 Macrophage Polarization via PTEN/PI3Kγ to Promote Pancreatic Cancer Metastasis. Cancer Res. *78*, 4586–4598.
44. Xue, M., Chen, W., Xiang, A., Wang, R., Chen, H., Pan, J., Pang, H., An, H., Wang, X., Hou, H., and Li, X. (2017). Hypoxic exosomes facilitate bladder tumor growth and development through transferring long non-coding RNA-UCA1. Mol. Cancer *16*, 143.
45. Hu, J.L., Wang, W., Lan, X.L., Zeng, Z.C., Liang, Y.S., Yan, Y.R., Song, F.Y., Wang, F.F., Zhu, X.H., Liao, W.J., et al. (2019). CAFs secreted exosomes promote metastasis and chemotherapy resistance by enhancing cell stemness and epithelial-mesenchymal transition in colorectal cancer. Mol. Cancer *18*, 91.
46. Clark, K.R., and Veale, B.L. (2018). Strategies to Enhance Data Collection and Analysis in Qualitative Research. Radiol Technol *89*, 482CT–485CT.
47. Wang, H.T., Tong, X., Zhang, Z.X., Sun, Y.Y., Yan, W., Xu, Z.M., and Fu, W.N. (2019). MYCT1 represses apoptosis of laryngeal cancerous cells through the MAX/miR-181a/NPM1 pathway. FEBS J. *286*, 3892–3908.
48. Xiong, W., Deng, H., Huang, C., Zen, C., Jian, C., Ye, K., Zhong, Z., Zhao, X., and Zhu, L. (2019). MLL3 enhances the transcription of PD-L1 and regulates anti-tumor immunity. Biochim. Biophys. Acta Mol. Basis Dis. *1865*, 454–463.
49. Guo, L., Wang, X., Yang, Y., Xu, H., Zhang, Z., Yin, L., Wang, Y., Yang, M., Zhao, S., Bai, S., et al. (2018). Methylation of DACT2 contributes to the progression of breast cancer through activating WNT signaling pathway. Oncol. Lett. *15*, 3287–3294.
50. Xia, M., Ling, F., Gao, F., and Tao, C. (2019). MLL3 promotes the senescence of esophageal squamous cell carcinoma. OncoTargets Ther. *12*, 1575–1582.
51. Zhao, Y., Wang, L., Ren, S., Wang, L., Blackburn, P.R., McNulty, M.S., Gao, X., Qiao, M., Vessella, R.L., Kohli, M., et al. (2016). Activation of P-TEFb by Androgen Receptor-Regulated Enhancer RNAs in Castration-Resistant Prostate Cancer. Cell Rep. *15*, 599–610.
52. Wang, Z.F., Liao, F., Wu, H., and Dai, J. (2019). Glioma stem cells-derived exosomal miR-26a promotes angiogenesis of microvessel endothelial cells in glioma. J. Exp. Clin. Cancer Res. *38*, 201.